Engineered Science
DOI: https://dx.doi.org/10.30919/es1300

Comparison of Treatment Positions for Tibia Fractures Using the External Narrow Locking Compression Plate: 3D Finite Element Analysis

Suwipong Hemathulin,[1] Direk Nualsing,[2,*] Nattadon Pannucharoenwong,[2,*] Kriengkrai Nabudda,[3,*] Permsak Paholpak,[4] Snunkhaem Echaroj[2] and Parramet Kongthip[2]

Abstract

Using an external fixation plate for the treatment of tibia fractures is a method of managing bone injuries that allows the patient to experience minimal trauma and a faster recovery time. When using the finite element to help analyze the stiffness, stress, strain, and deformation of movement that occurs. It will help determine the direction of treatment better. The study aims to evaluate the effect of treatment positions for tibia fractures using the External Narrow Locking Compression Plate (NLCP): 3D Finite Element Analysis. Tibia and fibula bone models were created for photorealism, and the materials employed in the simulation were linearly elastic, homogeneous, and isotropic. The model cuts 3 mm of space in the tibia. An average human body weight of 800 N is applied as a distributed load on the proximal tibia and fixed support at the distal tibia. The NLCP is installed in 3 areas: anterior, medial, and lateral. It can be concluded that treating tibia fractures with an external fixation installation on the anterior side will result in the highest stiffness of 164.90 N/mm and the least von-Miss stress of 2498.0 MPa. The strain is minimal at 0.6078, and the deformation of the osteotomy site is minimal at 4.8514 mm. This study demonstrates that installing the NLCP in the anterior region provides the most suitable results.

Keywords: Narrow locking compression plate; Tibia fractures; von Mises stress; Total deformation; Displacement.
Received: 11 September 2024; Revised: 12 October 2024; Accepted: 25 October 2024.
Article type: Research article.

1. Introduction

Recent advancements in external fixation for tibia fractures, particularly with the introduction of narrow locking compression plates (NLCP), mark a significant innovation. The tibia's crucial function in weight-bearing, combined with the intricate anatomy nearby, makes fractures demanding to manage, resulting in the development of a refined locking compression plate (LCP). This sophisticated device is designed to provide stable fixation, promoting faster recovery. Compared to traditional techniques, the innovation offers benefits such as reduced soft tissue damage, increased biomechanical stability, and enhanced fracture healing.

Researchers recommend a simulation-based optimization algorithm for refining the selection of implants and screw configurations in treating long bone fractures. The collaboration between LCP and external fixation, combining academic research with practical applications, equips orthopedic surgeons with an efficient toolset for handling fractures. Bone cement augmentation does increase construct stiffness; however, the dual-locking plate configuration, especially the lateral-medial setup, delivers the highest level of femur fixation stability under axial compression and lateral bending forces. Another study highlights the importance of

[1] *Department of Mechanical and Industrial, Faculty of Industrial Technology, Sakon Nakhon Rajabhat University, Sakon Nakhon 47000, Thailand.*
[2] *Department of Mechanical Engineering, Faculty of Engineering, Thammasat School of Engineering, Thammasat University, Bangkok 12120, Thailand.*
[3] *Department of Mechanical Engineering, Faculty of Engineering, Chiangrai College, Chiang Rai 57000, Thailand.*
[4] *Department of Orthopaedic, Faculty of Medicine, Khon Kaen University, Khon Kaen 40002, Thailand.*
**Email:* pnattado@engr.tu.ac.th (N. Pannucharoenwong), direk.nu@gmail.com (D. Nualsing), kriang.36@gmail.com (K. Nabudda)

bone cement augmentation in preventing implant failure in femoral allograft reconstruction.[1]

In clinical application, a study examines the efficacy of external LCPs in treating open ulnar and radial shaft fractures, highlighting benefits like low trauma, ease of use, dependable fixation, and improved forearm joint stability and function.[2] Findings reveal a significantly reduced time to union in the NLCP cohort, indicating potential for quicker recovery. In a distinct biomechanical analysis, tibia-LCPs have been found to provide unmatched stability against axial and torsional stresses, critical for the successful healing of tibia fractures.[3] The study also explores the potential for surgical site infection (SSI) and the necessity of reoperation within a year after implementing LCP, distal anatomical LCP, or a one-third tubular plate.[4] To improve surgical outcomes, the study proposes a simulation-based optimization algorithm to select the most optimal LCP and screw sets for treating long bone fractures.

Studies investigating the biomechanics of syndesmotic fixation techniques for ankle injuries evaluate the stiffness of endo button versus screw fixation post-syndesmotic injury with an ankle fracture, employing cadaveric validation and finite element analysis (FEA).[5,6] The research advises against forceful translation and compression during endobutton fixation, recommending a uniform rehabilitation regimen for both fixation techniques. LCPs used as low-profile external fixators (LPEF) show promise in addressing tibia fractures with compromised soft tissues, offering an improvement over conventional, uncomfortable external fixators.[7] This case series evaluates the effectiveness of LPEF, highlighting its potential for streamlined design, patient comfort, and positive outcomes, especially in soft tissue healing and resolving infections.[8-11] The crucial component of effective fracture healing, interfragmentary flexibility, is compared with predictions for maximum healing performance for implants, confirming the effectiveness of the proposed approach.[12-15]

Treating tibial fractures poses challenges due to complexity and potential complications. External fixation, a commonly used method, provides stability and support during healing. Recent advancements in orthopedics embrace FEA as a valuable tool for optimizing external fixation in tibia fractures, allowing a comprehensive assessment of biomechanical factors. Beyond biomechanical advantages,[16,17] a detailed analysis highlights the lower risks of infection and misalignment associated with NLCPs.[18-21] This is attributed to the procedure's minimal intrusion and improved fixation, emphasizing the need to incorporate innovative methods, including narrow LCPs, to optimize patient outcomes in managing tibia fractures.[22,23] In conclusion, integrating NLCP guidelines with FEA presents a robust framework for determining the suitability of external fixation devices for tibial surgery. By accurately predicting the stiffness of these devices, FEA enables a personalized and scientifically grounded approach to treatment. This methodology not only aligns with the NLCP's emphasis on individualized care but also enhances the overall success rates of external fixation surgeries. Ongoing research should aim to improve these predictive models and extend their application to additional types of orthopedic surgeries.

This study employs finite element methods to analyze damage in medical surgery, specifically concentrating on the 10-hole NLCP. The stiffness value is compared to the accepted criterion of the unilateral method for medical treatment. The unilateral method for treating a tibia fracture typically involves using a unilateral external fixation device. This method is often employed in cases of open fractures, complex fractures, or when internal fixation is not feasible due to soft tissue damage or infection risk. The unilateral external fixator is a device placed outside the body that stabilizes the fracture by using pins. The pins are attached to a rigid external frame, which keeps the bone fragments in the correct alignment. If the researched stiffness value surpasses that of the unilateral method,[24] it will be applied in the treatment of midshaft tibia fractures. The application of finite elements to help analyze models and evaluate treatment results is becoming popular and widely used today.[25]

2. Methods

2.1 Three-dimensional modeling

The tibia and fibula bone model was created from 2D computerized tomography (CT) scan images. The CT scan images were 0.5 mm thick in a 512×512 matrix. A three-dimensional tibia and fibula bone prototype was created using the software Mimics. A computer-aided design (CAD) software was employed to construct 3D models of the narrow locking compression with plate and screws (SolidWorks 2021). The tibia external fixation model includes a 10-hole NLCP plate with specific dimensions: a length of 192 mm, a hole distance of 20.0 mm, a thickness of 5 mm, and a width of 14 mm, and it is positioned 47 mm from the bone. The 10-hole NLCP size is suitable for basic treatment and is widely used. The screws, as illustrated in Fig. 1, have a diameter of 5 mm and a length of 73 mm. Additionally, the tibia length measures 449 mm, the median radius is 24 mm, and there is a 3.0 mm gap on the mid-shaft for the implant model. A distance of 3 mm is the maximum distance of the tibial bone gap that can be fused together, so it was determined in this simulation, as illustrated in Fig. 2.

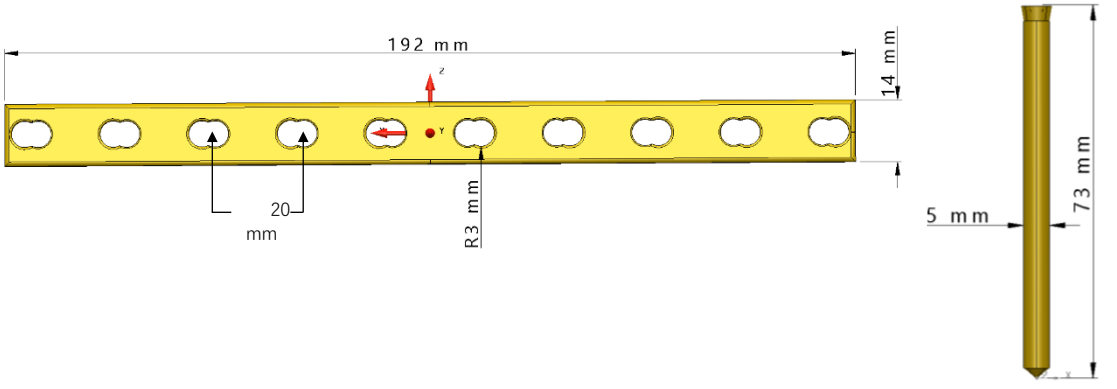

Fig. 1 3D model of narrow locking compression plate and screw.

The simulation process was diligently executed after the model generation, employing the ANSYS Workbench software, an advanced computational tool developed by ANSYS Company Inc., headquartered in Canonsburg, Pennsylvania, USA. This methodological approach aligns with contemporary practices in the field, ensuring precision and reliability in the analytical procedures applied to the study.

2.2 Finite element analysis

Once the tibia was properly aligned and a central cut was made, a 3 mm gap formed, and the NLCP was affixed to the tibia using a total of 10 screws. The NLCP covered the entire tibia and featured three sides: lateral, medial, and anterior. To evaluate the stiffness and tension, an 800 N force was applied, determined by the patient's weight, with the tibia's base secured in place. It was assumed that materials employed in the simulation were linearly elastic, homogeneous, and isotropic, with the tibia Young's modulus set at 805 MPa and a Poisson's ratio of 0.3. For the NLCP and screws, made from Stainless Steel 304 LVM, Young's modulus was specified as 195 GPa and the Poisson's ratio as 0.31. The Posteroinferior tibiofibular ligament had a Young's modulus of 88.82 MPa and a Poisson's ratio of 0.495.[26,27] In this study, the meshed system utilized belonged to a quadratic family of ten-node tetrahedral elements, which is suitable for biomechanical analysis.

2.3 Mechanical equations

The finite element method (FEM) is a numerical approach frequently employed to resolve intricate engineering problems, with a particular focus on structural analysis.[28] In the context of modeling tibia external fixation using FEM, a relevant mathematical model is designed, with the necessary equations determined by aspects like material properties, geometry, and loading conditions. A simplified finite element formulation for tibia external fixation involves a general structural equation based on force equilibrium, commonly expressed in linear elastic analysis.

$$K.U = F \tag{1}$$

In this context, K (N/mm) represents the stiffness matrix in Equations (1), U (m) denotes the displacement vector, and F (N) signifies the force vector. The cross-sectional bending stiffness EI is calculated by integrating Young's modulus, E (Pa), with the cross-sectional moment of inertia, I.[29,30] This relationship is expressed in Equations (2,3). Importantly, EI is derived from lateral bending stiffness, which is experimentally measured using four-point bending tests.

$$k = \frac{48EI}{L^3} \tag{2}$$

$$EI = \frac{kL^3}{48} \tag{3}$$

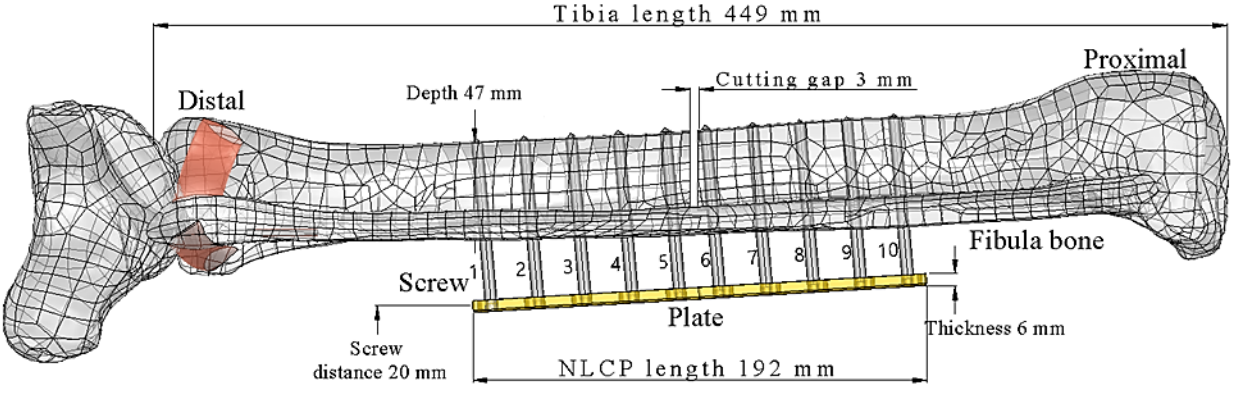

Fig. 2 3D assembly external fixation method for midshaft tibia fractures.

In this context, L (m) represents the distance between the supports, E (Pa) stands for the material's elastic modulus, and I (m^4) is the moment of inertia for the cross-section. The stiffness matrix integrates the properties of the material, including Poisson's Ratio (υ) and Young's Modulus (E). The constitutive matrix (D) for isotropic linear elastic solid materials is given by the following Equations (4). Ten-node quadratic tetrahedral elements are commonly used for meshing in bone simulations because they offer several advantages in capturing the complex geometry and behavior of biological tissues like bones. Quadratic elements have mid-side nodes, allowing for a more accurate approximation of curved surfaces and gradients compared to higher-order interpolation, enabling better representation of the stress and strain distribution in the complex geometry of bones.[31] Most finite element analysis (FEA) software, which is used for simulating the biomechanical behavior of bones, supports 10-node quadratic tetrahedral elements and can efficiently solve the governing differential equations involved in bone mechanics. The ten-node quadratic tetrahedral elements mesh, more accurate stress and strain fields, and efficient computational performance in capturing the intricate structure and behavior of bones under various loading conditions were utilized to establish 3D finite components using mesh conditions and the convergence test for meshing system proceeded at the node location shown in Fig. 3.[32,33]

$$D = \frac{E}{(1+\nu)(1-2\upsilon)} = \begin{bmatrix} 1-\upsilon & \upsilon & \upsilon & 0 & 0 & 0 \\ \upsilon & 1-\upsilon & \upsilon & 0 & 0 & 0 \\ \upsilon & \upsilon & 1-\upsilon & 0 & 0 & 0 \\ 0 & 0 & 0 & \frac{1-2\upsilon}{2} & 0 & 0 \\ 0 & 0 & 0 & 0 & \frac{1-2\upsilon}{2} & 0 \\ 0 & 0 & 0 & 0 & 0 & \frac{1-2\upsilon}{2} \end{bmatrix} \quad (4)$$

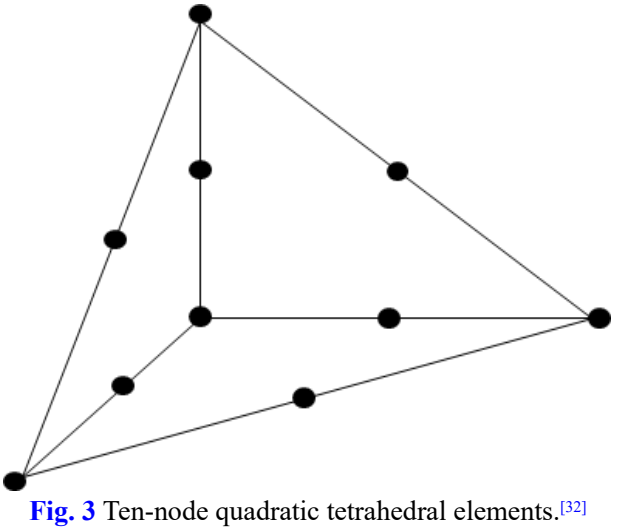

Fig. 3 Ten-node quadratic tetrahedral elements.[32]

To calculate the internal fixation implant's equivalent volume V (m^3), the following equation is applied in Equations (5).

$$V = L \times S \quad (5)$$

The soft tissue effect can be modeled as a stretch scenario, with S (m^2) as the cross-sectional area of the internal fixation and L (m) as its unit thickness. The direction of strain ε is illustrated below in Equations (6).[34,35]

$$\varepsilon = \frac{\Delta V}{L \times S} \quad (6)$$

The volume change ΔV (m^3), which can occur with or without internal fixation, is demonstrated here. The equation above describes the tissue's tensile balance force in Equations (7).

$$F = \sigma \times A \quad (7)$$

F is the compression force (N), σ demonstrates the stress (Pa) within the segment, and A (m^2) corresponds to the soft tissue's cross-sectional area; the equation is given in Equations (8).

$$F = E \times A \times \varepsilon \quad (8)$$

combining (8) and (6) gives in Equations (9).

$$F = E \times A \times \frac{\Delta V}{L \times S} \quad (9)$$

Equivalent von Mises stress of the tibial epiphyseal narrow locking compression plate was calculated with the following Equation (10).[36,37]

Von Misses Stress =

$$\sqrt{\frac{1}{2}[(\sigma_1 - \sigma_2)^2 + (\sigma_2 - \sigma_3)^2 + (\sigma_3 - \sigma_1)^2]} \quad (10)$$

The equivalent strain of the tibial epiphyseal narrow locking compression plate was calculated with the following Equation (11).[38]

$$\varepsilon_{eq} = \frac{2}{3}\sqrt{\frac{3}{2}(e_{xx}^2 + e_{yy}^2 + e_{zz}^2) + \frac{3}{4}(\gamma_{xy}^2 + \gamma_{yz}^2 + \gamma_{zx}^2)} \quad (11)$$

where deviatoric strains e are defined as Equations (12-14).[38]

$$e_{xx} = \frac{2}{3}\varepsilon_{xx} - \frac{1}{3}\varepsilon_{yy} - \frac{1}{3}\varepsilon_{zz} \quad (12)$$

$$e_{yy} = -\frac{1}{3}\varepsilon_{xx} + \frac{2}{3}\varepsilon_{yy} - \frac{1}{3}\varepsilon_{zz} \quad (13)$$

$$e_{zz} = -\frac{1}{3}\varepsilon_{xx} - \frac{1}{3}\varepsilon_{yy} + \frac{2}{3}\varepsilon_{zz} \quad (14)$$

2.4. Boundary conditions

The force applied to the proximal tibia was determined from the weight of the patients in the case study. The proximal tibia and proximal tibiofibular were fully bonded using a cylindrical model to provide distributed force. The model applied a compressive load of 800 N to the upper surface of tibiofibular, which was distributed across the proximal tibia

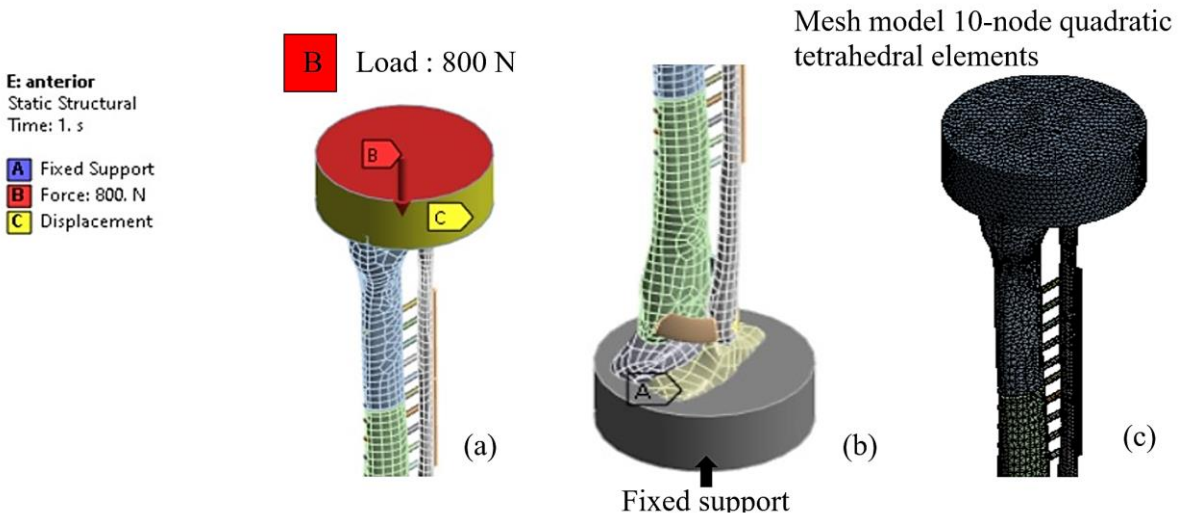

Fig. 4 Boundary conditions (a) distributed load (b) Fixed support (c) 10-node quadratic tetrahedral.

and proximal tibiofibular joints, as shown in Fig. 4a. Fixed support was placed at the distal tibia and distal tibiofibular joints, were fully bonded using a cylindrical model to provide fixed supported, as depicted in Fig. 4b. In the future, we will perform simulation tests using a Universal Testing Machine (UTM) using a bone clamp made of 304 stainless steel attached to an adapter. This material was chosen because it is resistant to oxidation when exposed to blood. The 10-hole NLCP model was bonded with a screw to be installed into the tibia. The 3-dimensional models in finite form, shown in Fig. 4c, were divided into meshes of 10-node quadratic tetrahedral elements.[39] Table 1 shows the material properties of the components in this model, which consist of the tibia bone, NLCP (stainless 304 LVM), Screw (stainless 304 LVM), Posteroinferior tibiofibular ligament, Interosseous ligament, and Anteroinferior tibiofibular ligament.

Table 1. The material properties selected for the implant model.[26,39]

Component	Young's Modulus (MPa)	Poisson's Ratio
Tibia Bone	805	0.30
NLCP (ST 304 LVM)	193000	0.31
Screw (ST 304 LVM)	110,000	0.33
Posteroinferior tibiofibular ligament	88.82	0.495
Interosseous ligament	120.58	0.495
Anteroinferior tibiofibular ligament	51.63	0.495

2.5. Mesh test analysis

Convergence analyses were carried out to identify appropriate mesh revisions. The mesh convergence analysis was conducted using a model of an intact tibia. By using the optimization method and convergence analysis, the finite element model was improved.[40,41] To investigate the relationship between stress and element size, a mesh test was run. With an element size of 5 mm, the ten-node tetrahedral elements mesh technique produced 222,566 elements and 328,238 nodes. In comparison to the other dimensions, the conventional stress tolerance is more in the middle, as Fig. 5 illustrates. As a result, 5 mm was selected as the element size for the calculations used in the development of the replacement model. In Fig. 6, the flow chart outlines the finite element analysis procedure employed to calculate the appropriate stiffness for tibial external fixation with a narrow locking compression plate.

3. Results and Discussion

The use of NLCP in external fixation has emerged as a promising strategy for treating tibial fractures, according to recent research findings. These studies offer valuable insights into the clinical outcomes associated with NLCP application. In a prospective cohort study, NLCP demonstrated notable stiffness, leading to a substantial reduction in the time required for union compared to traditional fixation methods. The study underscored the biomechanical advantages of NLCP, emphasizing its capacity for providing secure fixation.

In Fig. 7, the boundary condition involves the application of an 800 N axial compressive load. The displacement along the y-axis is treated as independent, while the displacements along the x- and z-axes are constrained to zero, consistent with the test conditions. Additionally, the distal tibia is rigidly fixed to prevent any movement. Fig. 7a shows the specified boundary condition of normal tibia bone. Fig. 7b shows the specified boundary condition, which involves applying axial compression for external fixation on the lateral side. In Fig. 7c,

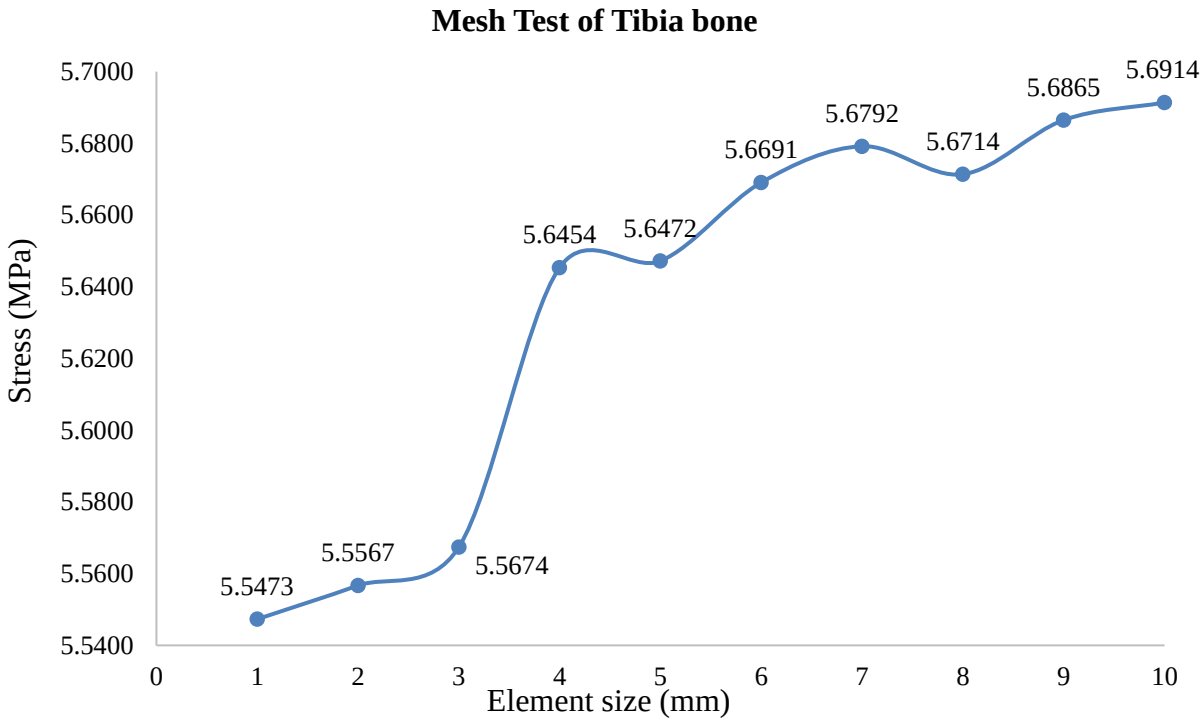

Fig. 5 An analysis of the mesh testing for the tibia bone.

the specified boundary condition involves applying axial compression for external fixation on the medial side. Fig. 7d shows the specified boundary condition, which involves applying axial compression for external fixation on the anterior side.

Structural properties are characterized by the stiffness value, which is determined by the slope of the force-displacement relationship. Fig. 8a illustrates this correlation between applied force and resulting displacement. Specifically, the stiffness of a normal tibia bone is quantified as 1096.94 N/mm. It has the highest stiffness value because it is a complete bone without any fractures or damage. Fig. 8b shows how this metric highlights the connection between force and displacement. The lateral side stiffness of the external fixation is specifically quantified at 123.00 N/mm. In Fig. 8c elucidates the connection between force and displacement. The medial side stiffness of the external fixation is determined to be 153.80 N/mm. As depicted in Fig. 8d, this metric clarifies the relationship between force and displacement. The stiffness on the anterior side of the external fixation is measured at 164.90 N/mm. From the installation model, this aspect gives the highest stiffness value.

The maximum von Mises stress resulting from compression load, shown in Fig. 9, highlights the possible damage to the model. For a normal tibia bone, the maximum stress is 100.51 MPa, as shown in Fig. 9a. In Fig. 9b, lateral fixation side, the maximum von Mises stress on the screw is 3737.9 MPa It shows that the screw area tends to break first, which has not affected the NLCP plate yet, and the screw can be repaired. In Fig. 9c, medial fixation side, the maximum von Mises stress on the screw is 2920.1 MPa. The von Mises stress that occurs will be less than the lateral fixation side. In Fig. 9d, anterior fixation side, the maximum von Mises stress on the screw is 2498.0 MPa. On this anterior fixation side, there will be the least amount of von Mises stress, which is important for the doctor to consider treatment to cause minimal damage to the NLCP and shin bones.

Figure 10 shows the maximum strain on the ligament. In Fig. 10a, the maximum strain on the ligament is 0.0893. Fig. 10b, lateral fixation side, illustrates the maximum strain on the ligament as 1.0472. Fig. 10c, medial fixation side, the ligament exhibits a maximum strain of 1.2319. Fig.10d, anterior fixation side, the ligament portrays a maximum strain of 0.6078. It can be seen that the stress generated will occur in the ligament. This is a point that is not related to the point where the NLCP is installed, and this area is a group of ligaments that can support elastic forces well.

Figure 11 shows the total deformation from the compression load. Fig. 11a, in normal tibia bone, reveals the maximum deformation on the fibula as 0.7293 mm. Fig. 11b, lateral fixation side, reveals the maximum deformation on the fracture area of the tibia bone as 6.5038 mm. Fig. 11c, medial

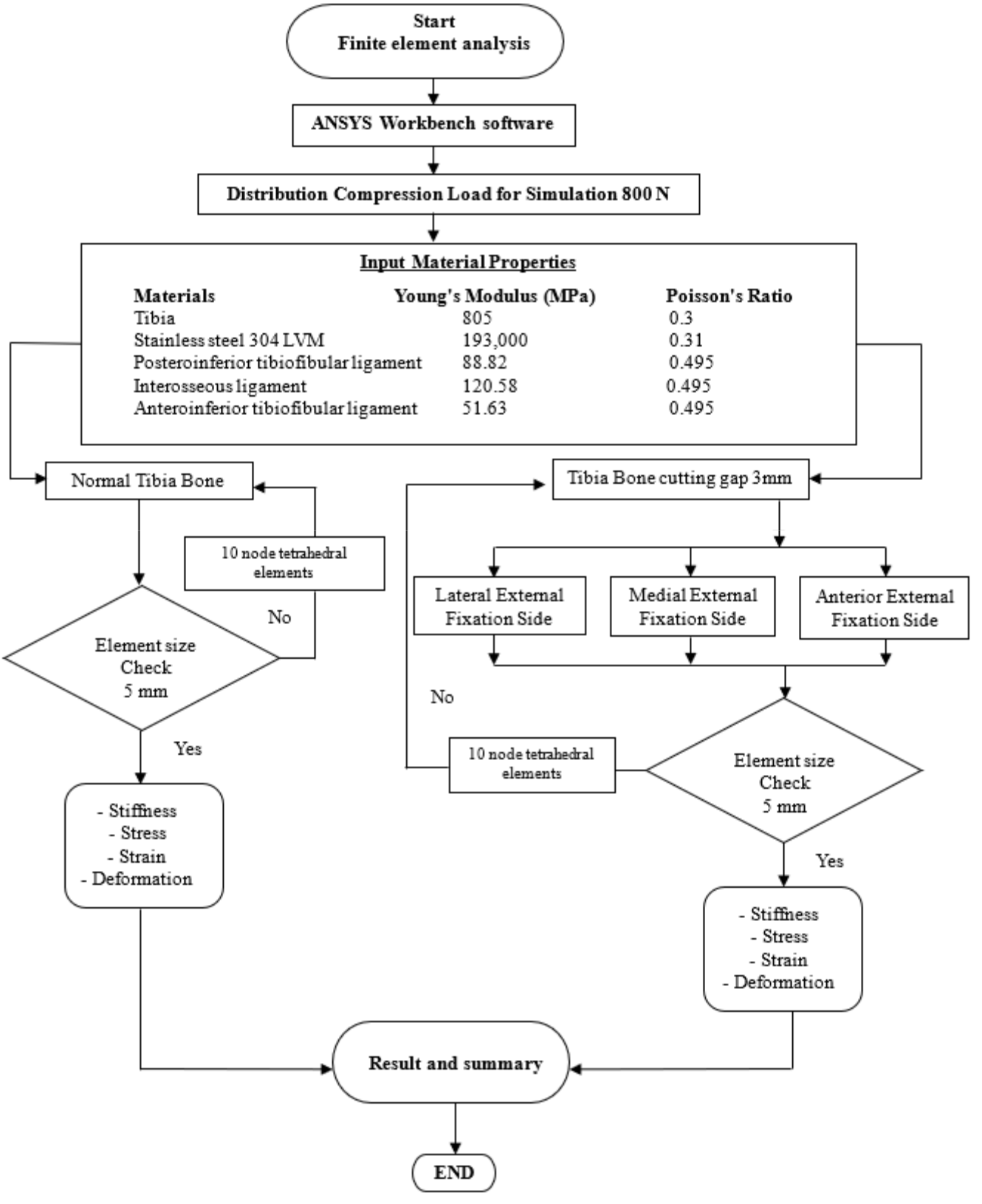

Fig. 6 Flow diagram of calculating for external fixation of the tibia using NLCP.

fixation side, the maximum deformation on the fracture area of the tibia bone is 5.2016 mm. Fig. 11d, anterior fixation side, the maximum deformation on the fracture area of the tibia bone is 4.8514 mm. Installing NLCP on the anterior fixation side appears to reduce overall deformation.

This research aimed to evaluate the influence of treatment

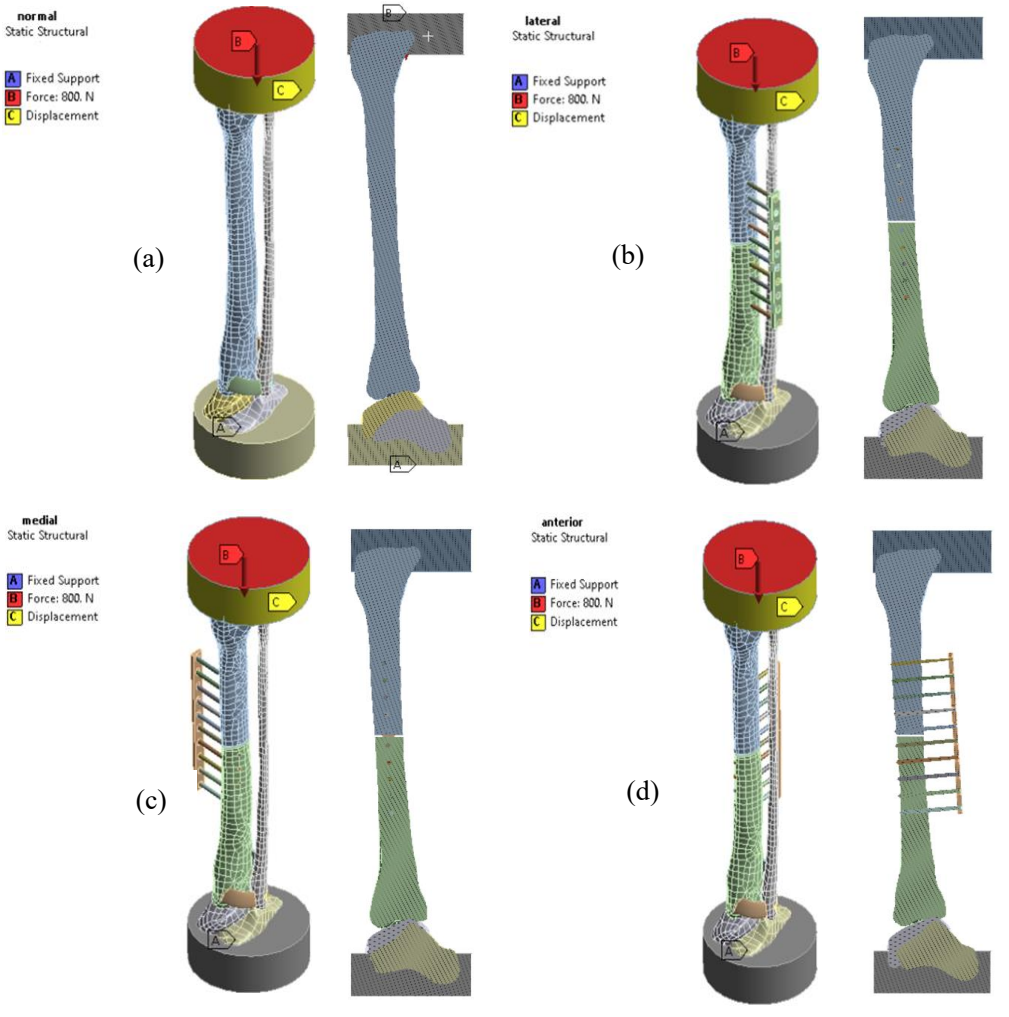

Fig. 7 Boundary condition applying an axial compression load; (a) normal tibia bone with cross-section view. (b) external fixation on the lateral side with a cross-section view. (c) external fixation on the medial side with a cross-section view. (d) external fixation on the anterior side with a cross-section view.

positions for tibia fractures using the External Narrow Locking Compression Plate (NLCP): 3D Finite Element Analysis. The results and discussion surrounding external fixation using NLCP for tibial fractures highlight promising clinical outcomes and biomechanical advantages. Academic studies provide a foundation for understanding the efficacy and potential complications associated with this technique. The ongoing exploration of external fixation methods contributes valuable insights to the orthopedic community, encouraging a nuanced approach to fracture management based on patient-specific factors and the evolving landscape of surgical techniques.

The stiffness is shown in Fig. 12. When the plate was installed on the anterior external fixation side, the stiffness value was 164.9 N/mm. On the medial external fixation side, it was 153.8 N/mm. And on the lateral external fixation side, it was the lowest at 123 N/mm. In comparison to the previous experiment, the stiffness value achieved in this experiment was 121.1 N/mm.[27] The stiffness value obtained in this study was highest when the NLCP was installed on the anterior side and was higher than in previous experiments. Due to the conditions of the 3D finite element analysis, we added a fibular model to make it as close to reality as possible.[42]

Taking into account the Maximum von Mises stress, as seen in Fig. 13, which will impact NLCP and tibia damage. The maximum von Mises stress value, 3737.9 MPa, was obtained when the NLCP was installed on the lateral external fixation side. The anterior external fixation side measured 2498 MPa, while the medial external fixation side measured a lower 2920.1 MPa. It can be seen that installation on the anterior external fixation side will cause the least amount of damage. And the point of damage will be around the screw used to hold it. If damage occurs to the screw, it can be quickly and easily fixed. However, when compared with past studies, it was found that the values obtained were different. Because previous studies have used different models, the von Mises

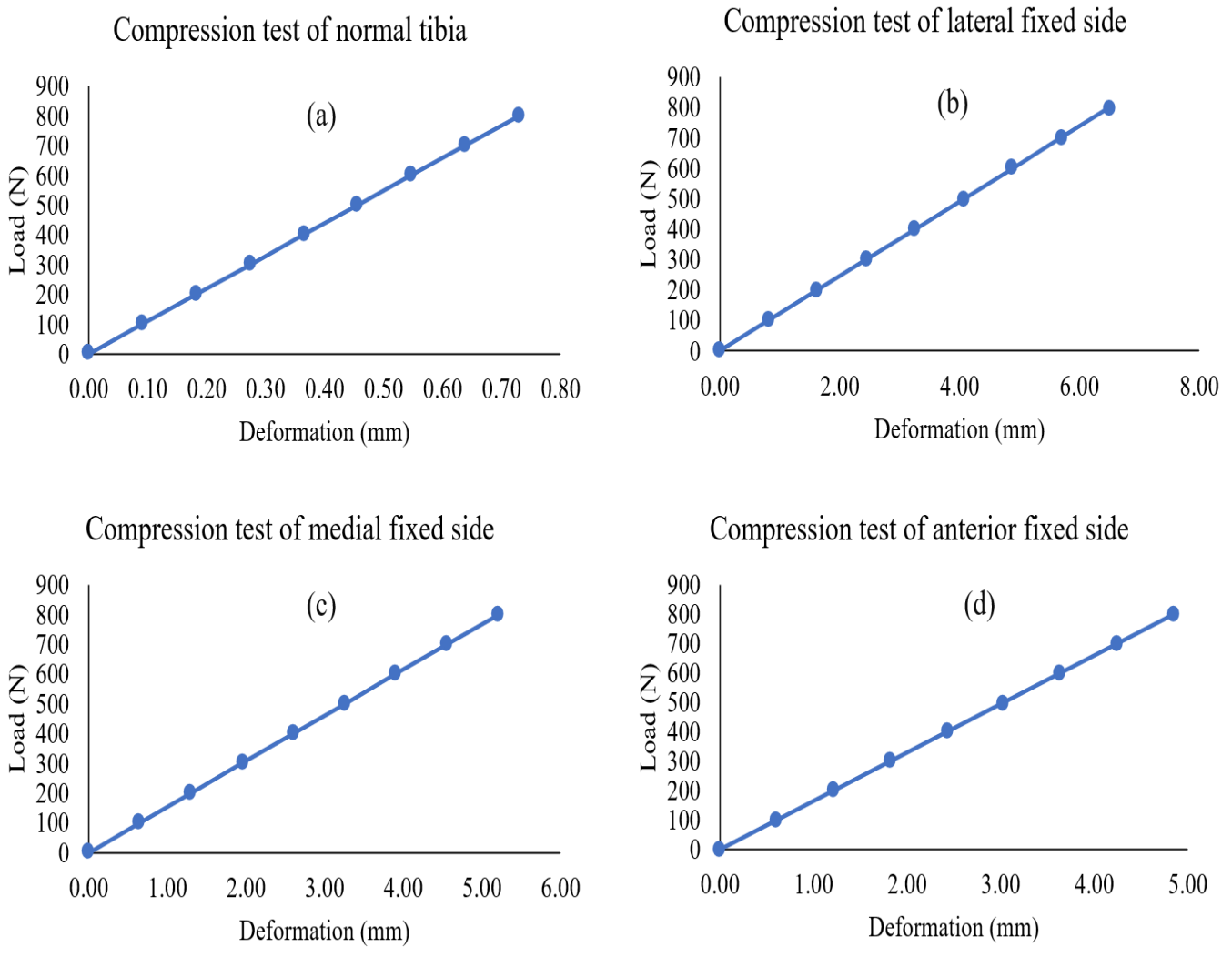

Fig. 8 Stiffness relationship between load and deformation; (a) stiffness normal tibia bone. (b) stiffness on the lateral side. (c) stiffness on the medial side. (d) stiffness on the anterior side.

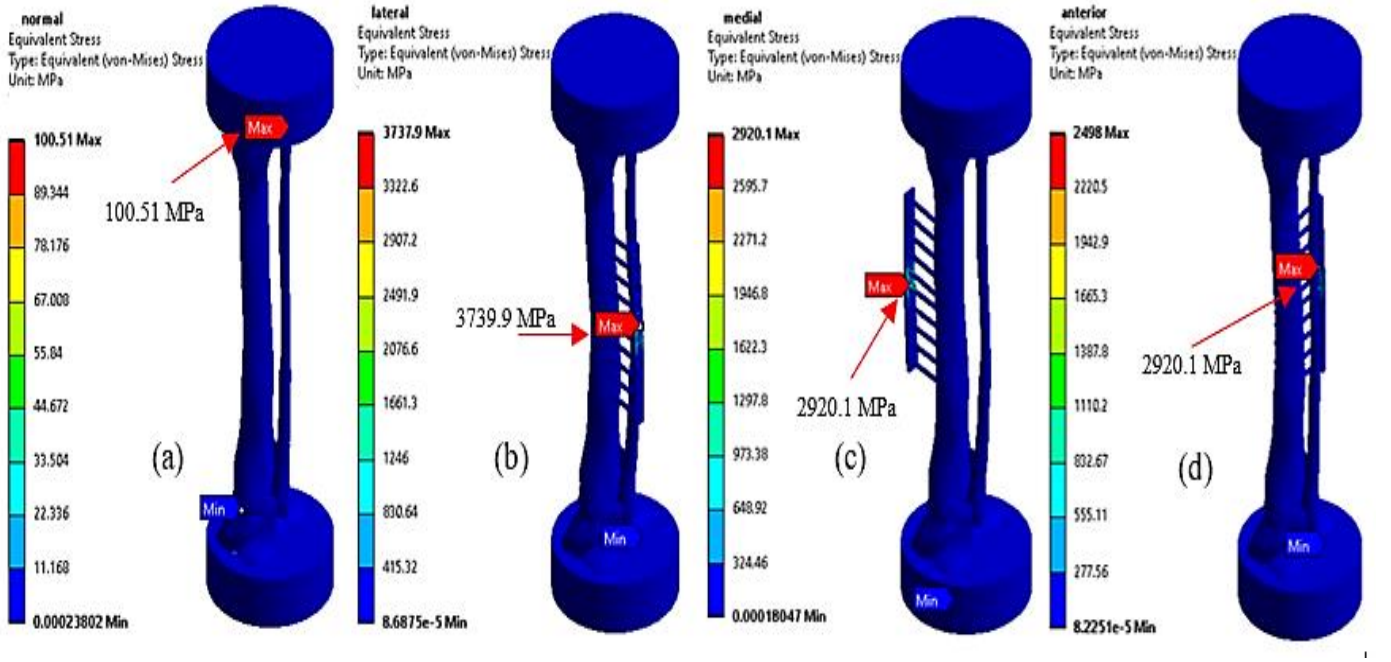

Fig. 9 Von-Mises stress; (a) Von-Mises stress on normal tibia bone. (b) Von-Mises stress on the lateral side. (c) Von-Mises stress on the medial side. (d) Von-Mises stress on the anterior side.

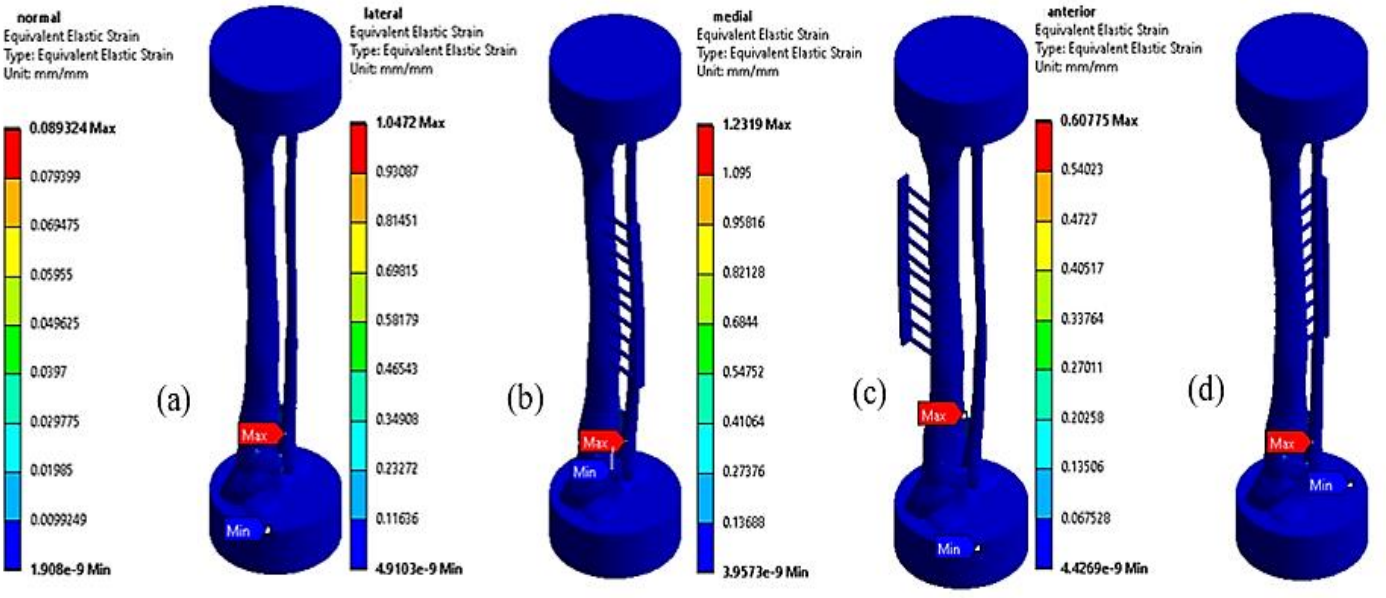

Fig. 10 Strain from compression load; (a) Strain on normal tibia bone. (b) Strain on the lateral side. (c) Strain on the medial side. (d) Strain on the anterior side.

stress value is lower than that of this study. This study created a model that is as close to reality as possible. A model of the fibula was added to provide the most realistic analysis of the model.

The strain values obtained from the analysis are shown in Fig. 14, when installed on the anterior external fixation side, the strain value was 0.6078, which is the lowest value. On the medial external fixation side, the strain value was 1.2319. Finally, when installed on the lateral external fixation side, the strain value was 1.0472, which is the maximum. When compared with the results of past studies, it was found that the strain values were similar when the NLCP was installed on the anterior side.

Strain is also related to the deformation of the material. In this study, the deformation occurred at the tibia cut site. This is in accordance with the predicted hypothesis because the area of the bone cut can cause the greatest internal deformation. It has been proved that in this study, the model can predict the outcome with high accuracy. The fibula model used in this analysis resulted in a deformation value that was as close to the real deformation as possible because, in the actual treatment, the fibula is still included in the patient's body as usual. When installed on the anterior external fixation side, the deformation value was 4.8514 mm, which is the lowest value shown in Fig. 15. When compared with previous studies, similar values were found.

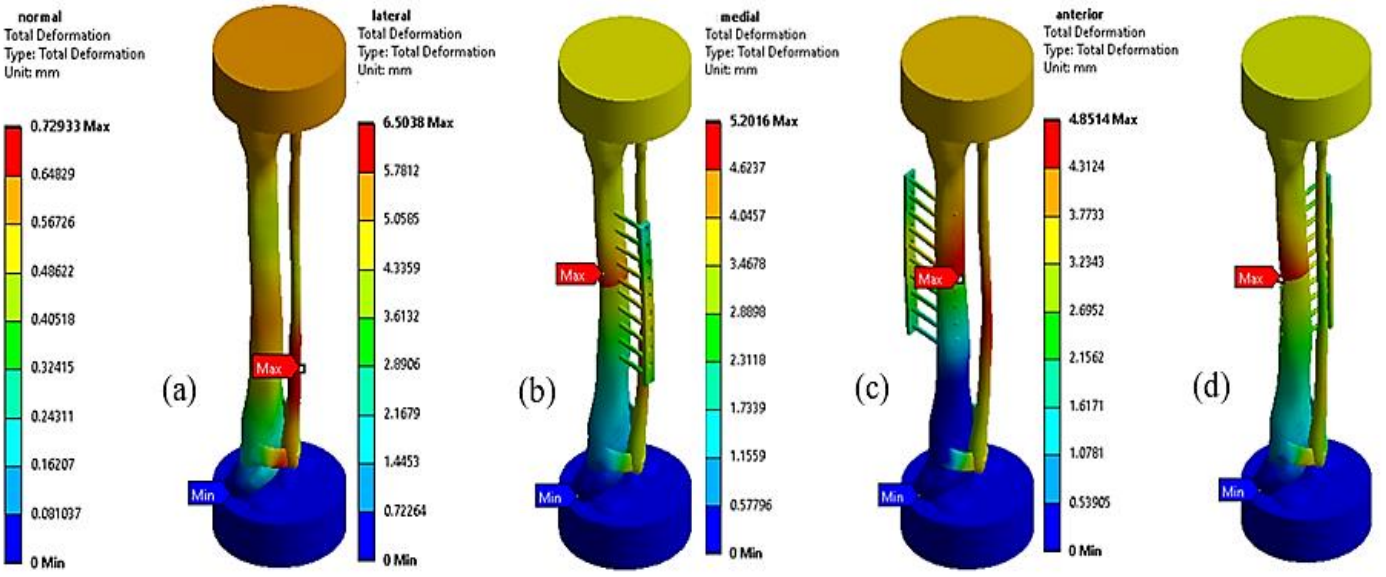

Fig. 11 Total deformation; (a) deformation of the normal tibia bone. (b) deformation on the lateral side. (c) deformation on the medial side. (d) deformation on the anterior side.

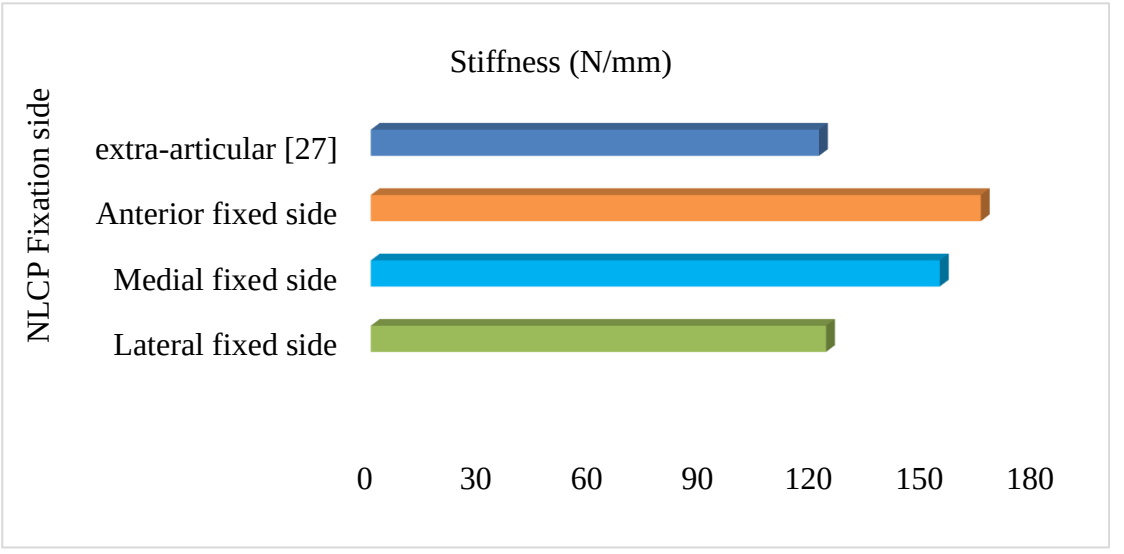

Fig. 12 Stiffness on NLCP for external fixation.

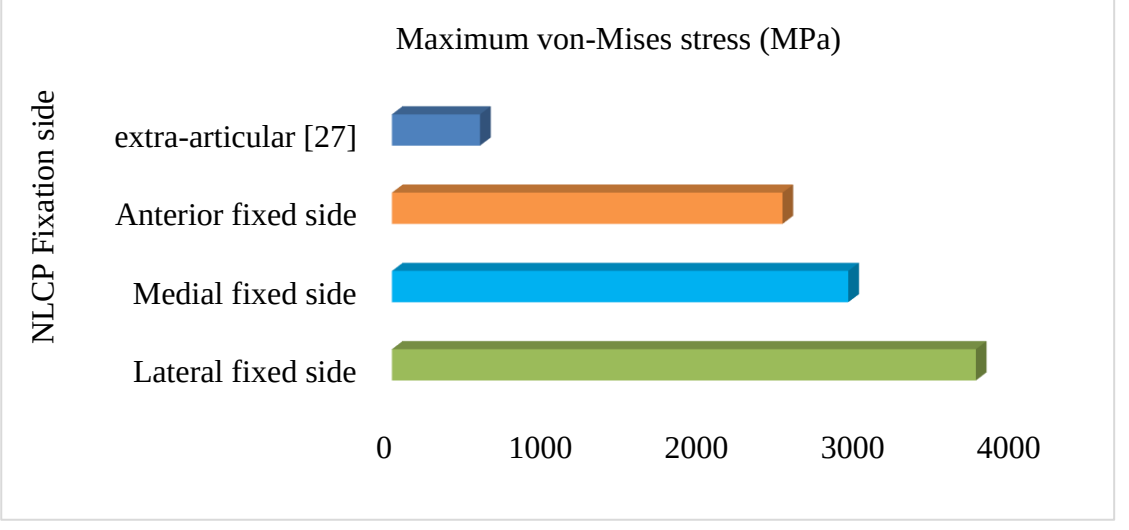

Fig. 13 Stress on NLCP for external fixation.

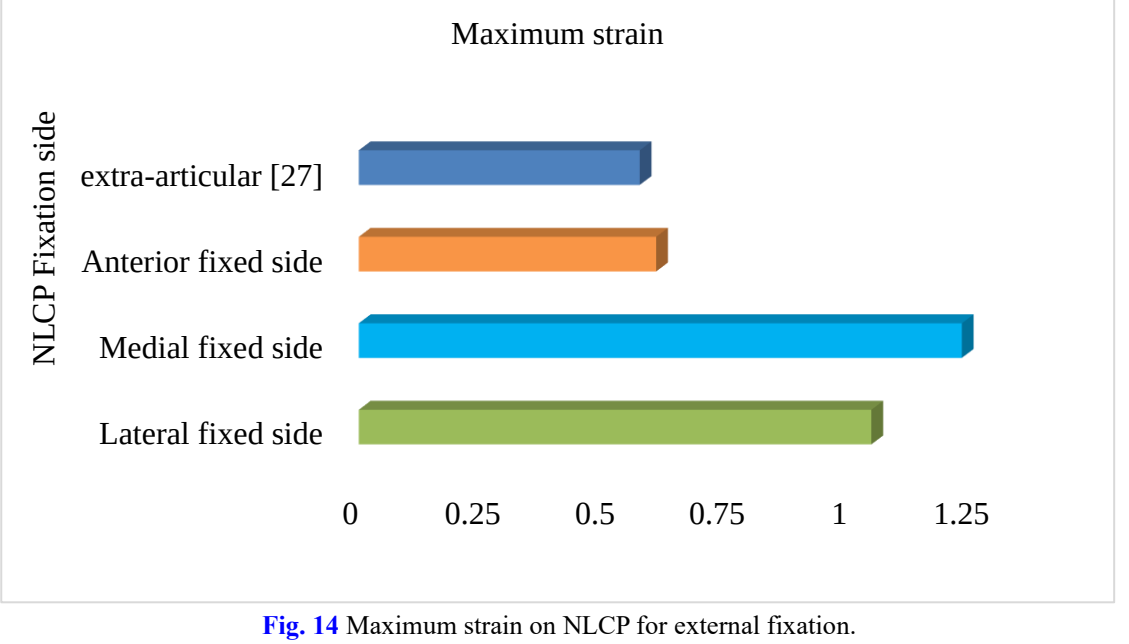

Fig. 14 Maximum strain on NLCP for external fixation.

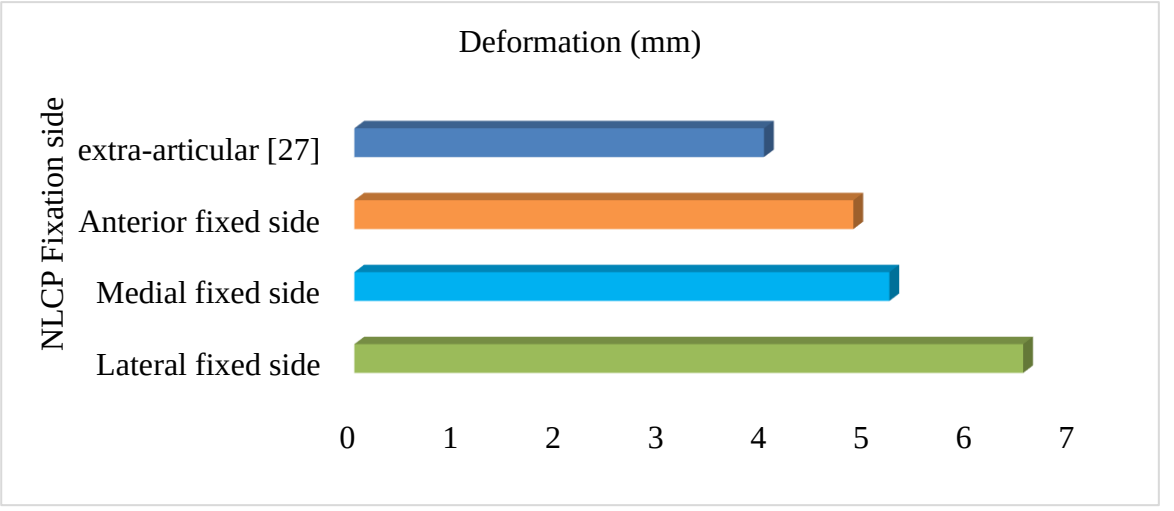

Fig. 15 Total deformation on NLCP for external fixation.

4. Conclusion

This study used 3D finite element analysis to investigate stiffness, stress, strain, and deformation for the treatment of tibia fractures. Simulating the biomechanics of tibia treatment is very important. It will help make the treatment more effective and accurate. A recent study indicates that implementing NLCP in external fixation presents a promising strategy for the treatment of tibial fractures. Choosing the position for installing the NLCP is extremely important because it can help increase stiffness, reduce stress and strain, and reduce the deformation that will occur. This study demonstrates how the selection of the NLCP installation position on each side can affect treatment. The critical focus on reevaluating NLCP for anterior external fixation forces is supported by academic studies utilizing finite element analysis to gain valuable insights into its performance. Furthermore, our findings highlight the need for further investigation of the various components of treatment to learn more about the complex aspects that influence the success of tibial fracture treatment.

Acknowledgements

Funding for this work was provided by the Thailand Science Research and Innovation Fundamental Fund for the fiscal year 2025, the Thammasat University Research Fund (Contract No TUFT 35/2567), and the Department of Mechanical and Industrial, Faculty of Industrial Technology, Sakon Nakhon Rajabhat University, Thailand. The authors are deeply grateful to the Department of Orthopaedics, Faculty of Medicine, Khon Kaen University, Thailand, for their ongoing support throughout the research project.

Conflict of Interest

There is no conflict of interest.

Supporting Information

Not applicable.

References

[1] K. Nabudda, J. Suriyawanakul, K. Tangchaichit, W. Kosuwon, K. Sukhonthamarn, N. Pannucharoenwong, Possibility of locking compression plate as the treatment of external fixation for femoral bone based on finite element method, *International Journal of Mechanical Engineering and Robotics Research*, 2023, **12**, 290-296, doi: 10.18178/ijmerr.12.5.290-296.

[2] T. Wisanuyotin, P. Paholpak, W. Sirichativapee, W. Sirichativapee, W. Kosuwon, Effect of bone cement augmentation with different configurations of the dual locking plate for femoral allograft fixation: finite element analysis and biomechanical study, *Journal of Orthopaedic Surgery and Research*, 2023, **18**, 405, doi: 10.1186/s13018-023-03894-3.

[3] T. Giver Jensen, M. Aqeel Khudhair Almadareb, M. Booth Nielsen, E. Jesper Hansen, M. Lindberg-Larsen, Outcome after treatment of distal fibula fractures using one-third tubular plate, locking compression plate or distal anatomical locking compression plate, *The Journal of Foot and Ankle Surgery*, 2023, **62**, 524-528, doi: 10.1053/j.jfas.2022.12.008.

[4] R. Rostamian, M. Silani, S. Ziaei-Rad, B. Busse, M. Qwamizadeh, T. Rabczuk, A finite element study on femoral locking compression plate design using genetic optimization method, *Journal of the Mechanical Behavior of Biomedical Materials*, 2022, **131**, 105202, doi: 10.1016/j.jmbbm.2022.105202.

[5] P. Meekaew, P. Paholpak, T. Wisanuyotin, W. Sirichativapee, W. Sirichativapee, W. Kosuwon, Y. Kasai, Biomechanics comparison between endobutton fixation and syndesmotic screw fixation for syndesmotic injury ankle fracture; a finite element analysis and cadaveric validation

study, *Journal of Orthopaedics*, 2022, **34**, 207-214, doi: 10.1016/j.jor.2022.08.019.
[6] M. Mühling, M. Winkler, P. Augat, Prediction of interfragmentary movement in fracture fixation constructs using a combination of finite element modeling and rigid body assumptions, *Computer Methods in Biomechanics and Biomedical Engineering*, 2021, **24**, 1752-1760, doi: 10.1080/10255842.2021.1919883.
[7] S. Ghimire, S. Miramini, G. Edwards, R. Rotne, J. Xu, P. Ebeling, L. Zhang, The investigation of bone fracture healing under intramembranous and endochondral ossification, *Bone Reports*, 2021, **14**, 100740, doi: 10.1016/j.bonr.2020.100740.
[8] M. Ernst, H. Baumgartner, S. Döbele, D. Höntzsch, T. Pohlemann, M. Windolf, Clinical feasibility of fracture healing assessment through continuous monitoring of implant load, *Journal of Biomechanics*, 2021, **116**, 110188, doi: 10.1016/j.jbiomech.2020.110188.
[9] T. Wisanuyotin, W. Sirichativapee, P. Paholpak, W. Kosuwon, Y. Kasai, Optimal configuration of a dual locking plate for femoral allograft or recycled autograft bone fixation: a finite element and biomechanical analysis, *Clinical Biomechanics*, 2020, **80**, 105156, doi: 10.1016/j.clinbiomech.2020.105156.
[10] A. Mehboob, S. H. A. Rizvi, S.-H. Chang, H. Mehboob, Comparative study of healing fractured tibia assembled with various composite bone plates, *Composites Science and Technology*, 2020, **197**, 108248, doi: 10.1016/j.compscitech.2020.108248.
[11] R. Kolasangiani, Y. Mohandes, M. Tahani, Bone fracture healing under external fixator: investigating impacts of several design parameters using Taguchi and ANOVA, *Biocybernetics and Biomedical Engineering*, 2020, **40**, 1525-1534, doi: 10.1016/j.bbe.2020.09.007.
[12] H. Ketata, M. Kharrat, M. Dammak, Modeling age-related changes in the mechanical behavior of the fracture-fixated human tibia bone during healing, *Medical Engineering & Physics*, 2020, **81**, 77-85, doi: 10.1016/j.medengphy.2020.05.011.
[13] A. H. Abdul Wahab, N. B. Wui, M. R. Abdul Kadir, M. H. Ramlee, Biomechanical evaluation of three different configurations of external fixators for treating distal third tibia fracture: finite element analysis in axial, bending and torsion load, *Computers in Biology and Medicine*, 2020, **127**, 104062, doi: 10.1016/j.compbiomed.2020.104062.
[14] S. Miramini, L. Zhang, M. Richardson, P. Mendis, A. Oloyede, P. Ebeling, The relationship between interfragmentary movement and cell differentiation in early fracture healing under locking plate fixation, *Australasian Physical & Engineering Sciences in Medicine*, 2016, **39**, 123-133, doi: 10.1007/s13246-015-0407-9.
[15] S. Zahaf, Study of the mechanical behavior of disc prostheses in the spine, 2018.
[16] N. Thapa, M. Prayson, T. Goswami, A failure study of a locking compression plate implant, *Case Studies in Engineering Failure Analysis*, 2015, **3**, 68-72, doi: 10.1016/j.csefa.2015.03.004.
[17] M. Elmedin, A. Vahid, P. Nedim, R. Nedžad, Finite element analysis and experimental testing of stiffness of the sarafix external fixator, *Procedia Engineering*, 2015, **100**, 1598-1607, doi: 10.1016/j.proeng.2015.01.533.
[18] B. Sepehri, E. Taheri, R. Ganji, Biomechanical analysis of diversified screw arrangement on 11 holes locking compression plate considering time-varying properties of callus, *Biocybernetics and Biomedical Engineering*, 2014, **34**, 220-229, doi: 10.1016/j.bbe.2014.05.001.
[19] H.-J. Kim, S.-H. Kim, S.-H. Chang, Finite element analysis using interfragmentary strain theory for the fracture healing process to which composite bone plates are applied, *Composite Structures*, 2011, **93**, 2953-2962, doi: 10.1016/j.compstruct.2011.05.008.
[20] F. Nabhani, E. J. Bradley, S. Hodgson, Comparison of two tools for the measurement of interfragmentary movement in femoral neck fractures stabilised by cannulated screws, *Robotics and Computer-Integrated Manufacturing*, 2010, **26**, 610-615, doi: 10.1016/j.rcim.2010.06.014.
[21] S.-H. Kim, S.-H. Chang, H.-J. Jung, The finite element analysis of a fractured tibia applied by composite bone plates considering contact conditions and time-varying properties of curing tissues, *Composite Structures*, 2010, **92**, 2109-2118, doi: 10.1016/j.compstruct.2009.09.051.
[22] B. Narayan, N. Giotakis, Stability with unilateral external fixation in the tibia, *Strategies in Trauma and Limb Reconstruction*, 2007, **2**, 13-20, doi: 10.1007/s11751-007-0011-y.
[23] P. Niemeyer, N. P. Südkamp, Principles and clinical application of the locking compression plate (LCP), *Acta Chirurgiae Orthopaedicae et Traumatologiae Cechoslovaca*, 2006, **73**, 221-228, doi: 10.55095/achot2006/032.
[24] L. Yang, S. Nayagam, M. Saleh, Stiffness characteristics and inter-fragmentary displacements with different hybrid external fixators, *Clinical Biomechanics*, 2003, **18**, 166-172, doi: 10.1016/s0268-0033(02)00175-4.
[25], S. Pai, N. Nayak, S. Awasthi, S. R. Acharya, V. Bhat, V. Patil, Effect of Thickness of Various Restorative Materials and Hybrid Layer on Stress Distribution of Direct Cervical Restorations of Teeth using a Three Dimensional Structural Finite Element Analysis, *Engineered Science*, 2021, **16**, 281-287, doi: 10.30919/es8d572.
[26] A. H. Abdul Wahab, N. B. Wui, M. R. Abdul Kadir, M. H. Ramlee, Biomechanical evaluation of three different configurations of external fixators for treating distal third tibia fracture: finite element analysis in axial, bending and torsion load, *Computers in Biology and Medicine*, 2020, **127**, 104062, doi: 10.1016/j.compbiomed.2020.104062.
[27] M. H. Ramlee, H. S. Gan, S. A. Daud, A. Abdul Wahab, M. R. Abdul Kadir, Stress distributions and micromovement of fragment bone of pilon fracture treated with external fixator:

a finite element analysis, *The Journal of Foot and Ankle Surgery*, 2020, **59**, 664-672, doi: 10.1053/j.jfas.2019.09.006.
[28] D. Blažević, J. Kodvanj, P. Adamović, D. Vidović, Z. Trobonjača, S. Sabalić, Comparison between external locking plate fixation and conventional external fixation for extraarticular proximal tibial fractures: a finite element analysis, *Journal of Orthopaedic Surgery and Research*, 2022, **17**, 16, doi: 10.1186/s13018-021-02907-3.
[29] O. Grundnes, O. Reikerås, Effects of instability on bone healing: Femoral osteotomies studied in rats, *Acta Orthopaedica Scandinavica*, 1993, **64**, 55-58, doi: 10.3109/17453679308994529.
[30] F. Chen, X. Huang, Y. Ya, F. Ma, Z. Qian, J. Shi, S. Guo, B. Yu, Finite element analysis of intramedullary nailing and double locking plate for treating extra-articular proximal tibial fractures, *Journal of Orthopaedic Surgery and Research*, 2018, **13**, 12, doi: 10.1186/s13018-017-0707-8.
[31] A. Chemmami, B. Aour, S. Zahaf, M. Dahmane, I. Bekkar, G. Mehdi, D. Boutchicha, Biomechanical Comparison of Three Total Artificial Discs: Sb-Charite III®, Prodisc-L® and Maverick® Reinforced By a Posterior Fixation System in the spinal column: A Three-Dimensional Finite Element Analysis, *Structural Integrity and Life*, 2021, **21**, 65-83.
[32] J. Zhang, N. Ebraheim, M. Li, X. He, J. Schwind, J. Liu, L. Zhu, External fixation using locking plate in distal tibial fracture: a finite element analysis, *European Journal of Orthopaedic Surgery & Traumatology*, 2015, **25**, 1099-1104, doi: 10.1007/s00590-015-1604-7.
[33] A. Mestar, S. Zahaf, N. Zina, A. Boutaous, Numerical study of the effect of elastomer and cement of stress absorbers on the reduction of stresses in tibia and tibial bone analysed by finite element method, *Nano Biomedicine and Engineering*, 2018, **10**, 56-78, doi: 10.5101/nbe.v10i1.p56-78.
[34] D. Schenk, M. Indermaur, M. Simon, B. Voumard, P. Varga, M. Pretterklieber, K. Lippuner, P. Zysset, Unified validation of a refined second-generation HR-pQCT based homogenized finite element method to predict strength of the distal segments in radius and tibia, *Journal of the Mechanical Behavior of Biomedical Materials*, 2022, **131**, 105235, doi: 10.1016/j.jmbbm.2022.105235.
[35] M. Wang, Y. Deng, P. Xie, J. Tan, Y. Yang, H. Ouyang, D. Zhao, G. Huang, W. Huang, Optimal design and biomechanical analysis of a biomimetic lightweight design plate for distal tibial fractures: a finite element analysis, *Frontiers in Bioengineering and Biotechnology*, 2022, **10**, 820921, doi: 10.3389/fbioe.2022.820921.
[36] J.-J. Zhou, M. Zhao, D. Liu, H.-Y. Liu, C.-F. Du, Biomechanical property of a newly designed assembly locking compression plate: three-dimensional finite element analysis, *Journal of Healthcare Engineering*, 2017, **2017**, 8590251, doi: 10.1155/2017/8590251.
[37] H. Watanabe, K. Murase, D. Kim, T. Matsumoto, T. Majima, A posterior tibial slope angle over 12 degrees is critical to epiphyseal fracture of the proximal tibia: three-dimensional finite element analysis, *Heliyon*, 2023, **9**, e18854, doi: 10.1016/j.heliyon.2023.e18854.
[38] B. Keddar, B. Aour, S. Zahaf, C. Boualem, Static study and finite element analysis of a new method of fixation of a medial humerus fracture by an intramedullary nailing system analyzed by the ANSYS workbench 16.2 calculus code, *Nano Biomedicine and Engineering*, 2019, **11**, 272-289, doi: 10.5101/nbe.v11i3.p272-289.
[39] I. Keddar, B. Aour, S. Zahaf, Comparative study of the fractured humerus fixation by intramedullary nailing and compression plate, *Journal of Failure Analysis and Prevention*, 2022, **22**, 1905-1923, doi: 10.1007/s11668-022-01459-w.
[40] S. Zahaf, S. Kebdani, Biomechanical study between the rigid and dynamic fixation systems of the spinal column analyzed by the finite element method, *Nano Biomedicine and Engineering*, 2017, **9**, 169-183, doi: 10.5101/nbe.v9i2.p169-183.
[41] S. Zahaf, S. Kebdani, Study and analysis of mechanical behavior between rigid and dynamic fixation systems analyzed by the finite element method, *Journal of Biomimetics, Biomaterials and Biomedical Engineering*, 2017, **33**, 12-31, doi: 10.4028/www.scientific.net/jbbbe.33.12.
[42] A. Mestar, S. Zahaf, N. Zina, A. Boutaous, Development and validation of a numerical model for the mechanical behavior of knee prosthesis analyzed by the finite elements method, *Journal of Biomimetics, Biomaterials and Biomedical Engineering*, 2018, **37**, 12-42, doi: 10.4028/www.scientific.net/jbbbe.37.12.

